

FATTENING IN TWO DIMENSIONS OBTAINED WITH A NONSYMMETRIC ANISOTROPY: NUMERICAL SIMULATIONS

M. PAOLINI

ABSTRACT. In this paper we present a few numerical simulations of a nonsymmetric anisotropic evolution by mean curvature which leads to the so-called **fattening** of the interface. The numerical simulations are based on a diffused interface approximation via a bistable reaction-diffusion equation which is then discretized by means of finite elements in space and forward differences in time. An adaptive strategy, together with the use of a dynamic mesh, is used to take advantage of the local behaviour of the equation at hand.

However, this particular choice of anisotropy, with a large ratio between the maximal and minimal surface energy, seems to be highly critical for the type of approximation presented here, leading to very expensive computations in terms of CPU time.

1. INTRODUCTION

Evolution of surfaces by their local mean curvature has been extensively studied by many authors ([3], [11], [15], [18], [21], [22], [23]).

The definition in terms of viscosity solutions of some degenerate parabolic equation, studied in [11], [15], [29], provides a generalization of the classical law which allows to continue the evolution past singularities in a unique way. In this approach the evolving surface is recovered as the zero level-set of an evolving function defined over the whole space. However, a nasty kind of singularity can appear, consisting in the so-called **fattening** of the interface, i.e. the zero level-set develops, just after the singularization time, an interior. In such situation, other generalized approaches, such as that proposed by Brakke in [9], lead to nonuniqueness of the evolution. In practical terms, we are in an unstable situation: small perturbations in the initial datum lead to completely different evolutions.

Determination of which initial data can lead to **fattening** is thus an important issue, which has been investigated e.g. in [4], [5], [25]; numerical simulations of fattening based on a diffused interface approximation can be found in [16].

It turns out that under pure mean curvature flow $V = -\kappa$, an initial regular, compact, embedded curve in \mathbf{R}^2 can never develop fattening. The very interesting example provided by Angenent, Chopp and Ilmanen in [4], show that in \mathbf{R}^3

Received November 17, 1997.

1980 *Mathematics Subject Classification* (1991 *Revision*). Primary 35K55; Secondary 65M99.

fattening of a **nice** initial surface is indeed (quite probably) possible, although the construction is not at all simple.

It is possible, however, to construct examples of fattening even in two dimensions if we generalize to some extent the pure law of motion $V = -\kappa$. For example, by the addition of a forcing term we can construct a simple example consisting of two evolving circles [6]. The effect of boundary conditions can also lead to fattening in an example proposed by Giga and presented (numerical simulations) in [16].

The purpose of this paper is to present some numerical simulation of **anisotropic** motion by mean curvature which, for a particularly selected initial curve, should lead to fattening. A theoretical proof of such behaviour is not yet published (to our knowledge), although it should not be difficult by using the same comparison arguments of [6]. For this example we chose a **nonsymmetric** anisotropy, which has the effect of leading to an evolution law which is not invariant under change of orientation of the surface; in this respect our example is very similar to that presented in [6].

Anisotropic motion by mean curvature is introduced in [8] as

$$(1.1) \quad \mathbf{v} = -\kappa_\phi \mathbf{n}_\phi,$$

where \mathbf{v} denotes the velocity vector, κ_ϕ and \mathbf{n}_ϕ are the anisotropic counterparts of the mean curvature κ and the unit normal ν respectively. Concerning anisotropic motion by mean curvature we also refer to [2], [13], [17], [19], [20], [31], [32]. In this paper we shall basically stick to the notations of [8], where motion by mean curvature is derived starting from an anisotropic version of surface energy, with density given by a given function $\phi^o(\nu)$, ν being the unit normal vector to the oriented surface. Anisotropic motion by mean curvature is then basically obtained as a gradient flow for such surface energy.

Our numerical simulations are based on a preliminar approximation of the **sharp interface** problem with a **diffused interface** version [1], where an approximation parameter $\epsilon > 0$ appears, which plays the role of **thickness** of the diffused interface. For pure motion by mean curvature one obtains the well known Allen-Cahn equation

$$(1.2) \quad \epsilon^2 \partial_t u_\epsilon - \epsilon^2 \Delta u_\epsilon + \psi(u_\epsilon) = 0$$

where $\psi = \frac{1}{2} \Psi'$ is the derivative of a double well potential with equal depths, the typical choice being $\Psi(t) := (1 - t^2)^2$.

Convergence of the Allen-Cahn equation (1.2) to evolution by mean curvature has been studied by many authors, see e.g. [10], [12], [14], [24], [26].

The anisotropic counterpart of (1.2) is introduced in [8] as

$$(1.3) \quad \epsilon^2 \partial_t u_\epsilon - \epsilon^2 \operatorname{div} T^o(\nabla u_\epsilon) + \psi(u_\epsilon) = 0$$

where the nonlinear transformation T^o is defined via

$$T^o(\xi) := \phi^o(\xi) \nabla_{\xi} \phi^o(\xi)$$

and ϕ^o is extended to non-unit vectors by positive one-homogeneity. A discretized version of (1.3) is discussed in [30], together with some numerical examples of anisotropic evolution. Such approach is also followed here; we also make use of the **dynamic mesh** method described in [28] with a density function for the graded mesh which concentrates the degrees of freedom near the location where the singularity will develop (which is known in advance).

This paper is organized as follows. In Section 2 we introduce the nonsymmetric anisotropy of our example and some basic notation; in Section 3 we present our fattening example; in Section 4 we show the results of a few numerical simulations, and finally draw some conclusions in Section 5.

2. ANISOTROPY DEFINITION AND NOTATIONS

We stick to the notation of [8]. The Finsler metric is defined by

$$\phi^o(x, \xi) = \phi^o(\xi) := |\xi| \psi(\theta), \quad \text{with } \psi(\theta) := 1 - A \sin \theta$$

where $0 \leq A < 1$ is a given parameter, and θ is the argument of the vector ξ , defined via $\xi = |\xi|(\cos \theta, \sin \theta)^t$. This Finsler metric can also be written in a more convenient way as

$$(2.1) \quad \phi^o(\xi) = |\xi| - A \xi_2$$

where ξ_2 is the second component of the vector $\xi = (\xi_1, \xi_2)^t$.

It is useful to define the two monotone transformations $S^o : \mathbf{R}^2 \setminus \{0\} \rightarrow \partial W_{\phi}$ and $T^o : \mathbf{R}^2 \rightarrow \mathbf{R}^2$ (the latter is the duality operator mapping the Frank diagram F_{ϕ} onto the Wulff shape W_{ϕ})

$$\begin{aligned} S^o(\xi) &:= \nabla_{\xi} \phi^o(\xi) = \frac{\xi}{|\xi|} - A \mathbf{e}_2 \\ T^o(\xi) &:= \phi^o(\xi) S^o(\xi), \end{aligned}$$

where \mathbf{e}_2 is the second element of the canonical basis: $\mathbf{e}_2 = (0, 1)^t$.

For any $\xi \in \mathbf{R}^2 \setminus \{0\}$ we have $|S^o(\xi) + A \mathbf{e}_2| = 1$, so that we conclude that W_{ϕ} is a circle of radius 1 centered at $(0, -A)^t$, i.e. $W_{\phi} = \mathcal{B}_1 - A \mathbf{e}_2$, where \mathcal{B}_1 denotes the unit circle

$$(2.2) \quad \mathcal{B}_1 = \{x \in \mathbf{R}^2 : |x| < 1\}.$$

On the contrary, $F_{\phi} = \{\xi \in \mathbf{R}^2 : \phi^o(\xi) < 1\}$ is not a circle, see Figure 2.1.

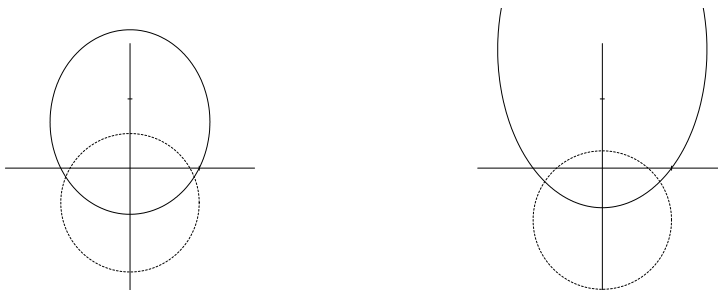


Figure 2.1. Frank diagram and Wulff shape for $A = 0.5$ and $A = 0.75$.

Once we know the shape of W_ϕ it is relatively easy to compute the Finsler metric ϕ (dual of ϕ°), which has to be positively homogeneous of degree 1. After some computations we get

$$\phi(\xi) = \frac{\sqrt{|\xi|^2 - A^2\xi_1^2} + A\xi_2}{1 - A^2}.$$

2.1. Consequences of the Nonsymmetry

The Finsler metric defined in (2.1) is clearly not symmetric. This has some consequences in the definition of relative curvature and relative motion by mean curvature. In particular, the evolution of an oriented surface $\Sigma(t)$, viewed as the boundary of its interior $I(t)$, does not coincide with the evolution of the same surface with the opposite orientation (the boundary of $\mathbf{R}^2 \setminus I(0)$).

For this reason, only oriented (with a specified interior) surfaces can be evolved. In the level set approach it is no longer true that any initial datum having Σ as zero level surface gives rise to the same evolution, rather, one has to restrict to initial data having a given sign (e.g. positive) in the interior of the surface.

2.2. Relative Curvature and Evolution

In two dimensions, the relative curvature κ_ϕ associated to a generic anisotropy can be computed as

$$\kappa_\phi = \kappa(\psi + \psi_{\theta\theta})$$

so that for the particular choice (2.1) of the metric, the relative curvature actually coincides with the euclidean curvature, since $\psi + \psi_{\theta\theta} = 1$. However, the evolution is not the same as the classical mean curvature flow, since we now have a different Cahn-Hoffmann vector $\mathbf{n}_\phi = T^\circ(\nu_\phi)$, with $\nu_\phi = \frac{\nu}{\phi^\circ(\nu)}$.

The fact that the relative curvature coincides with the euclidean curvature is consistent with the fact that the Wulff shape, which in our case is just a translated unit circle, always has relative curvature 1 (see [8]).

Under relative motion by mean curvature, we know that the Wulff shape shrinks selfsimilarly, with the law of motion

$$W(t) = \sqrt{1 - 2t}W_\phi,$$

from that, using the translation invariance of the evolution, we can compute the evolution of the circle $I_e := \Lambda\mathcal{B}_1$, where \mathcal{B}_1 is defined in (2.2) and $\Lambda > 0$, as

$$I_e(t) = \sqrt{\Lambda^2 - 2t}\mathcal{B}_1 + A \left[\Lambda - \sqrt{\Lambda^2 - 2t} \right] \mathbf{e}_2.$$

The circle drifts upwards while shrinking to the point $A\Lambda\mathbf{e}_2$ at time $t_e^* = \frac{\Lambda^2}{2}$.

We are now interested in determining the evolution of the complementary of a circle of radius λ , i.e. $I_i := \mathbf{R}^2 \setminus \lambda\mathcal{B}_1$, which is easily seen to satisfy

$$\mathbf{R}^2 \setminus I_i(t) = \sqrt{\lambda^2 - 2t}\mathcal{B}_1 - A \left[\lambda - \sqrt{\lambda^2 - 2t} \right] \mathbf{e}_2,$$

corresponding to a circle which drifts downward while shrinking to the point $-A\lambda\mathbf{e}_2$ at time $t_i^* = \frac{\lambda^2}{2}$.

3. EVOLUTION OF A RING

Given the two values $0 < \lambda < \Lambda$ we consider the set $I := \Lambda\mathcal{B}_1 \setminus \lambda\mathcal{B}_1$, and we denote by $I(t)$ the evolution of I by anisotropic mean curvature, in the sense of the level-set approach [11], or in the sense of De Giorgi's barriers [7].

It is clear that the two connected components $\Sigma_e = \Lambda\partial\mathcal{B}_1$ and $\Sigma_i = \lambda\partial\mathcal{B}_1$ of ∂I will evolve independently with the laws of motion obtained in Section 2.2, as long as they do not intersect each other. Based on the ratio $r = \frac{\Lambda}{\lambda}$ we face two possible types of evolution:

1. If r is very large (thick ring), the internal circle will disappear before it could touch the evolving outer circle; in this case we have no merging of the two evolving circles and the exact evolution will be $I_e(t) \cap I_i(t)$ for $0 \leq t \leq t_i^*$; $I_e(t)$ for $t_i^* < t \leq t_e^*$; the empty set for $t > t_e^*$.
2. If r is sufficiently close to 1, then the two circles will touch at some point before the smaller one vanishes. This is clear, since they are focusing at two points which are quite far apart (independently of r). The exact evolution is known only before the touching time $t^c(r)$, and is given by $I_e(t) \cap I_i(t)$.

As a consequence, fattening is expected corresponding to some intermediate value r_* of r .

Let

$$\begin{aligned} g_e(t) &:= (1 + A)\sqrt{\Lambda^2 - 2t} - A\Lambda \\ g_i(t) &:= (1 - A)\sqrt{\lambda^2 - 2t} + A\lambda \end{aligned}$$

To compute the critical value for r , we shall track the motion of the two points $P_e(t) := (0, -g_e(t)) \in \Sigma_e(t)$ and $P_i(t) := (0, -g_i(t)) \in \Sigma_i(t)$. They are clearly the points that minimize the distance between $\Sigma_e(t)$ and $\Sigma_i(t)$, and the distance itself is simply given by $g_e(t) - g_i(t)$. The critical value r_* is then characterized by the fact that the two parabolas given by the graphs of g_e and g_i are tangential to each other. After a few computations (performed using MuPad) we finally get

$$r_* = \frac{4 + A}{4 - A}.$$

The critical time and the singularity position assume a particularly simple expression if we further impose $\Lambda + \lambda = 2$. For such choice we obtain $t^c = \frac{3}{32}(4 - A^2)$ and $P(t) = (0, -\frac{1}{4}(2 + A^2))$.

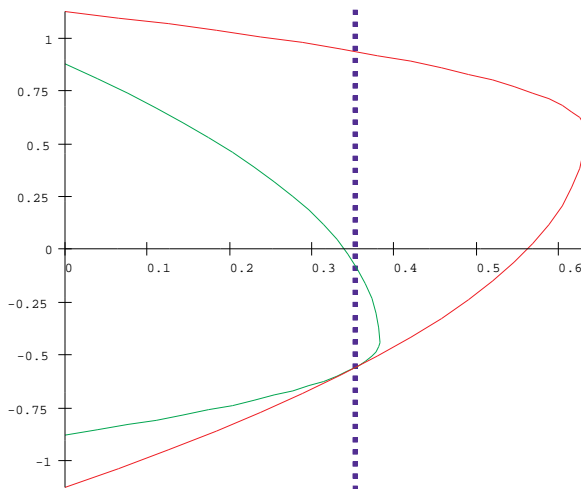


Figure 3.1. Evolution of the ring for $A = 0.5$ and $r = r_*$ (critical value), $\partial I(t) \cap \{x_1 = 0\}$ versus time and critical time $t = t^c$.

In Figure 3.1 we show the exact evolution of $\partial I_e \cap \{x_1 = 0\}$ (external curve) and $\partial I_i \cap \{x_1 = 0\}$ (internal curve) versus time corresponding to the choice $A = 0.5$, $\lambda = 1 - A/4 = 0.875$, $\Lambda = 1 + A/4 = 1.125$, i.e. $\lambda + \Lambda = 2$ and $r = r_*$. The two evolutions touch at the critical time $t = t^c = 0.3515625$ (vertical dashed line).

4. DISCRETIZATION AND NUMERICAL SIMULATIONS

4.1. Relaxation

The evolution equation (1.1) is first approximated by using a diffused interface model similar to (1.3), more precisely we consider the following reaction-diffusion equation

$$(4.1) \quad \epsilon a \partial_t u_\epsilon - \epsilon \operatorname{div} a T^o(\nabla u_\epsilon) + \frac{1}{a\epsilon} \psi(u_\epsilon) \ni 0$$

where $a: \mathbf{R}^2 \rightarrow \mathbf{R}^+$ is a given density function which allows to reduce the interfacial width near the location of the singularity. ψ here is the Frechet subdifferential of the double-well potential defined via

$$\Psi(t) := \begin{cases} 1 - t^2 & \text{if } |t| \leq 1, \\ +\infty & \text{otherwise.} \end{cases}$$

Convergence of such variant of the Allen-Cahn equation to motion by mean curvature is studied in [27] in the case of isotropic mean curvature flow (T^o is the identity).

4.2. Discretization

Following [30] we then discretize (4.1) via piecewise linear finite elements in space and forward differences in time. The finite element mesh is constructed based on the same density function $a(x)$ which is used in (4.1) in order to resolve the singularity formation.

The **dynamic mesh** strategy described in [28] is then used to obtain the final numerical code. As an example, in Figures 4.3 and 4.4 we present the dynamic mesh at $t = 0$ and $t = 0.35$ for one of the simulations of our example.

The introduction of the anisotropy in the **dynamic mesh** strategy requires however some attention. The initial datum for (4.1) should now be defined as

$$u_0(x) := \gamma \left(\frac{d_\phi}{\epsilon a} \right)$$

where γ is, as usual, a solution to the one-dimensional problem $-\gamma'' + \psi(\gamma) \ni 0$, which for our choice of the bistable potential gives $\gamma(t) = \sin(t)$ for $t \in (-\pi/2, \pi/2)$, and d_ϕ is the anisotropic counterpart of the usual signed distance function to the initial front. For a spatially homogeneous anisotropy, which is the case here, the anisotropic distance $\operatorname{dist}_\phi(x, y)$ between two points $x, y \in \mathbf{R}^2$ is given by $\phi(x - y)$ where ϕ is the dual norm to ϕ^o (see [8]). Now the signed distance d_ϕ can be defined as usual in terms of dist_ϕ .

4.3. Numerical simulations

Our numerical simulations are performed with the choice $A = 0.5$, $\lambda + \Lambda = 2$, and λ is the only free parameter, which we let vary in the interval $[0.86, 0.87]$ which contains the **discrete** critical value (we recall that the theoretically computed critical value for the continuous problem is $\lambda_* = 0.875$). We also fix $\epsilon = 0.0629956$ and $h = 0.015$. The density function a is of the form

$$a(x) = \sigma(|x - x_c|)$$

where $x_c = (0, 0.5625)$ and $\sigma(t) = \min(1, \max(0.1, \frac{2}{3}t))$.

By enforcing the symmetry of the example, we solve the problem on the domain

$$\Omega := (0, 3) \times (-3, 3)$$

with a reflection condition along the x_2 axis. The conditions on the other sides are irrelevant since the front will never meet them.

We shall present here the results of just two numerical simulations, corresponding to the (discrete) subcritical value $\lambda = 0.86$ and the (discrete) supercritical value $t = 0.87$.

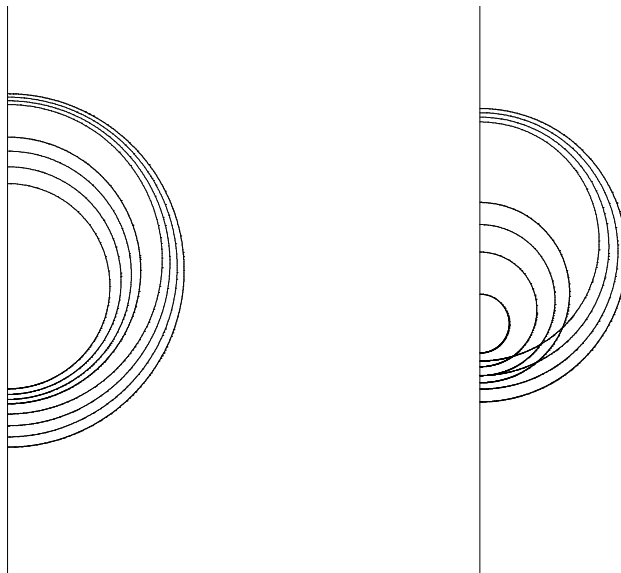


Figure 4.1. $\lambda = 0.86$, $t = 0 - 0.35$ step 0.05.

The results of the simulation for $\lambda = 0.86$ are presented in Figures 4.1 and 4.2 where the position of the discrete interface (zero level-set of the discrete solution) is shown at time intervals of 0.05. The small circle shrinks fast enough to avoid

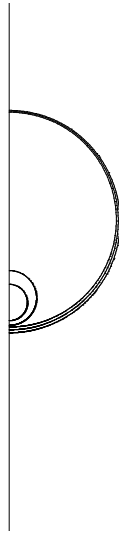


Figure 4.2. $\lambda = 0.86$, $t = 0.35 - 0.37$ step 0.01.

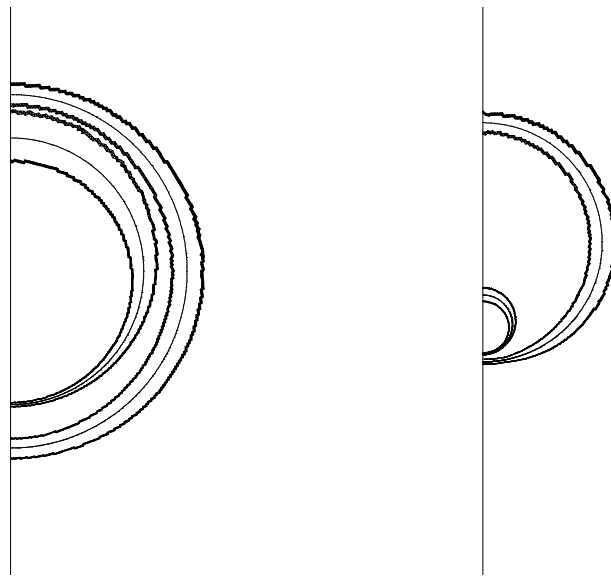


Figure 4.3. $\lambda = 0.86$. Dynamic mesh at $t = 0$ and some $t = 0.35$.
Only the boundary triangles of the transition region are depicted.

touching the larger circle and vanishes at some time between 0.36 and 0.37. The boundary elements of the dynamic mesh at times $t = 0$ and $t = 0.25$ is shown in Figures 4.3 and 4.4.

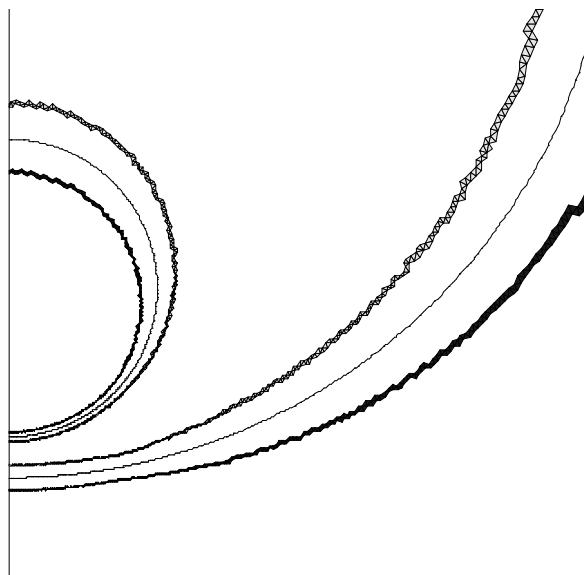


Figure 4.4. $\lambda = 0.86$. Zoom at $t = 0.35$.

The discrete interfaces obtained for the supercritical value $\lambda = 0.87$ is shown in Figures 4.5 and 4.6. The two circles touch each other at some time between 0.3 and 0.31. After that time the topology changes into a simply connected shape which slowly approaches the shape of a shrinking circle.

5. CONCLUSIONS

Each of the simulations presented here did require an incredibly long CPU time (of the order of some days of computation on a Pentium pro 200 processor). The reason for such long computation times is related to the thickness of the transition region for the diffused interface model. By performing a simple asymptotic expansion for the parabolic equation (4.1) one realizes that the shape of the solution across the interface is approximately given by

$$u(x, t) := \gamma \left(\frac{d_\phi(x, t)}{\epsilon a} \right).$$

It is apparent that, for a constant density a , the thickness will be uniform in terms of the anisotropic distance d_ϕ and correspondingly highly nonuniform in terms of the euclidean distance: for $A = 0.5$ the ratio will be 3 between the thickness corresponding to the normal $(0, 1)$ and to the normal $(0, -1)$. This effect is clear in Figure 4.3 by looking at the top part of the two transition regions (where a is constant equal to 1).

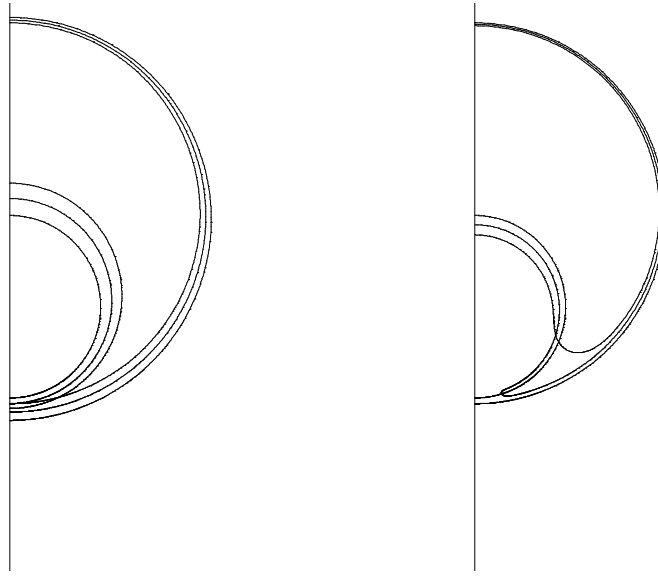


Figure 4.5. $\lambda = 0.87$, $t = 0.26, 0.28, 0.3$, and $t = 0.3, 0.31, 0.32$.

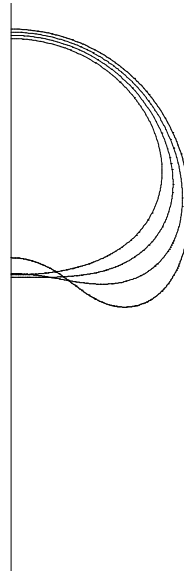


Figure 4.6. $\lambda = 0.87$, $t = 0.34 - 0.40$ step 0.02.

As a consequence the number of triangles across the interface varies of a factor of 3, which forces the choice of a very small mesh size to have enough triangles where the transition region is thin.

We could try to control the mesh size based on the orientation of the interface in order to keep a constant number of triangles across the interface, or we could change the density function a according to the orientation in order to balance the variations in d_ϕ so as to keep the transition width constant. As a result we shall run into problems whenever the transition regions of interfaces with opposite orientation intersect each other, which is quite possible and actually happens in our simulations for supercritical values of λ . In such a situation we shall either have triangles of very different size coming into contact, or, even worse, create a jump in space in the density function a .

For such reasons the use of the **diffused interface** model for this kind of non-symmetric anisotropy needs to be further investigated in order to become effective.

References

1. Allen S. M. and Cahn J. W., *A macroscopic theory for antiphase boundary motion and its application to antiphase domain coarsening*, Acta Metall. Mater. **27** (1979), 1085–1095.
2. Almgren F. and Taylor J. E., *Flat flow is motion by crystalline curvature for curves with crystalline energies*, J. Differential Geom. **42** (1995), 1–22.
3. Altschuler S., Angenent S. B. and Giga Y., *Mean curvature flow through singularities for surfaces of rotation*, J. Geom. Anal. **5** (1995), 293–358.
4. Angenent S. B., Chopp D. L. and Ilmanen T., *A computed example of nonuniqueness of mean curvature flow in R^3* , Comm. Partial Differential Equations **20** (1995), 1937–1958.
5. Angenent S. B., Ilmanen T. and Velasquez J., *Nonuniqueness of motion by mean curvature in dimensions four through seven*, in preparation.
6. Bellettini G. and Paolini M., *Two examples of fattening for the curvature flow with a driving force*, Atti Accad. Naz. Lincei Cl. Sci. Fis. Mat. Natur. Rend. (9) Mat. Appl. **5** (1994), 229–236.
7. ———, *Some results on minimal barriers in the sense of De Giorgi applied to driven motion by mean curvature*, Rend. Accad. Naz. Sci. XL Mem. Mat. (5) **19** (1995), 43–67.
8. ———, *Anisotropic motion by mean curvature in the context of Finsler geometry*, Hokkaido Math. J. **25** (1996), 537–566.
9. Brakke K. A., *The Motion of a Surface by its Mean Curvature*, Mathematical Notes, 20, Princeton University Press, Princeton, 1978.
10. Bronsard L. and Kohn R. V., *Motion by mean curvature as the singular limit of Ginzburg-Landau dynamics*, J. Differential Equations **90** (1991), 211–237.
11. Chen Y. G., Giga Y. and Goto S., *Uniqueness and existence of viscosity solutions of generalized mean curvature flow equations*, J. Differential Geom. **33** (1991), 749–786.
12. De Giorgi E., *Some conjectures on flow by mean curvature*, Methods of real analysis and partial differential equations (M. L. Benevento, T. Bruno, and C. Sbordone, eds.), Liguori, Napoli, 1990.
13. Dohmen C. and Giga Y., *Selfsimilar shrinking curves for anisotropic curvature flow equations*, Proc. Japan Acad. A **70** (1994), 252–255.
14. Evans L. C., Soner H.-M. and Souganidis P. E., *Phase transitions and generalized motion by mean curvature*, Comm. Pure Appl. Math. **45** (1992), 1097–1123.
15. Evans L. C. and Spruck J., *Motion of level sets by mean curvature. I*, J. Differential Geom. **33** (1991), 635–681.
16. Fierro F. and Paolini M., *Numerical evidence of fattening for the mean curvature flow*, Math. Models Methods Appl. Sci. **6** (1996), 793–813.

17. Fukui T. and Giga Y., *Motion of a graph by nonsmooth weighted curvature*, Proceedings of the First World Congress of Nonlinear Analysis 1 (V. Lakshmikantham, ed.), Gruyter, Berlin, 1995, pp. 47–56.
18. Gage M. E. and Hamilton R. S., *The heat equations shrinking convex plane curves*, J. Differential Geom. **23** (1986), 69–96.
19. Giga M.-H. and Giga Y., *Evolving graphs by singular weighted curvature*, Arch. Rational Mech. Anal., (to appear).
20. ———, *A subdifferential interpretation of crystalline motion under nonuniform driving force*, Dynamical Systems and Differential Equations (W. Chen and S. Hu, eds.), vol. I, 1998, pp. 276–287.
21. Grayson M. A., *The heat equation shrinks embedded plane curves to round points*, J. Differential Geom. **26** (1987), 285–314.
22. Huisken G., *Asymptotic behavior for singularities of the mean curvature flow*, J. Differential Geom. **31** (1990), 285–299.
23. Ilmanen T., *Generalized flow of sets by mean curvature on a manifold*, Indiana Univ. Math. J. **41** (1992), 671–705.
24. ———, *Convergence of the Allen-Cahn equation to Brakke’s motion by mean curvature*, J. Differential Geom. **38** (1993), 417–461.
25. ———, *Dynamics of stationary cones*, In preparation.
26. Nochetto R. H., Paolini M. and Verdi C., *Optimal interface error estimates for the mean curvature flow*, Ann. Scuola Norm. Sup. Pisa Cl. Sci. (4) **21** (1994), 193–212.
27. ———, *Double obstacle formulation with variable relaxation parameter for smooth geometric front evolutions: asymptotic interface error estimates*, Asymptotic Anal. **10** (1995), 173–198.
28. ———, *A dynamic mesh algorithm for curvature dependent evolving interfaces*, J. Comput. Phys. **123** (1996), 296–310.
29. Osher S. and Sethian J. A., *Fronts propagating with curvature dependent speed: algorithms based on Hamilton-Jacobi formulations*, J. Comput. Phys. **79** (1988), 12–49.
30. Paolini M., *An efficient algorithm for computing anisotropic evolution by mean curvature*, Curvature Flows and Related Topics, GAKUTO Internat. Ser. Math. Sci. Appl. (A. Damlamian *et al.*, eds.), Gakkōtoshō, Tokyo, 1995, pp. 199–213.
31. Roosen A. R. and Taylor J. E., *Modeling crystal growth in a diffusion field using fully faceted interfaces*, J. Comput. Phys. **114** (1994), 113–128.
32. Taylor J. E., *Mean curvature and weighted mean curvature II*, Acta Metall. Mater. **40** (1992), 1475–1485.

M. Paolini, Dipartimento di Matematica e Informatica, Università di Udine, 33100 Udine, Italy,
e-mail: paolini@dimi.uniud.it